Electronic Supplementary Material to: Changes in Global Vegetation Distribution and Carbon Fluxes in Response to Global Warming: Simulated Results from IAP-DGVM in CAS-ESM2*

Xiaofei GAO[1,2], Jiawen ZHU[1], Xiaodong ZENG[1,2,3], Minghua ZHANG[4], Yongjiu DAI[5], Duoying JI[6], and He ZHANG[1]

[1]*International Center for Climate and Environment Sciences*, *Institute of Atmospheric Physics*, *Chinese Academy of Sciences*, *Beijing* 100029, *China*

[2]*University of Chinese Academy of Sciences*, *Beijing* 100049, *China*

[3]*Collaborative Innovation Center on Forecast and Evaluation of Meteorological Disasters*, *Nanjing University of Information Science and Technology*, *Nanjing* 210044, *China*

[4]*School of Marine and Atmospheric Sciences*, *Stony Brook University*, *NY* 11790, *USA*

[5]*School of Atmospheric Sciences*, *Sun Yat-Sen University*, *Guangzhou* 510275, *China*

[6]*College of Global Change and Earth System Science*, *Beijing Normal University*, *Beijing* 100875, *China*

ESM to: Gao, X. F., J. W. Zhu, X. D. Zeng, M. H. Zhang, Y. J. Dai, D. Y. Ji, and H. Zhang, 2022: Changes in global vegetation distribution and carbon fluxes in response to global warming: Simulated results from IAP-DGVM in CAS-ESM2. *Adv. Atmos. Sci.*, **39**(8), 1285−1298, https://doi.org/10.1007/s00376-021-1138-3.

Table S1. Plant functional types (PFTs) in IAP-DGVM and their corresponding abbreviations in this study.

Plant functional types	Abbreviation
Needleleaf evergreen temperate tree	NEM
Needleleaf evergreen boreal tree	NEB
Needleleaf deciduous boreal tree	NDB
Broadleaf evergreen tropical tree	BET
Broadleaf evergreen temperate tree	BEM
Broadleaf deciduous tropical tree	BDT
Broadleaf deciduous temperate tree	BDM
Broadleaf deciduous boreal tree	BDB
Broadleaf evergreen shrub	BEsh
Broadleaf deciduous temperate shrub	BDMsh
Broadleaf deciduous boreal shrub	BDBsh
C3 arctic grass	C3Ar
C3 non-arctic grass	C3NA
C4 grass	C4

*The online version of this article can be found at 10.1007/s00376-021-1138-3.

Table S2. List of 16 models derived from CMIP5 used in this study.

Model name	References
ACCESS1.3	(Bi et al., 2013)
BCC-CSM1.1(m)	(Wu et al., 2014)
BCC-CSM1.1	(Wu et al., 2013)
CNRM-CM5	(Voldoire et al., 2012)
GFDL-CM3	(Griffies et al., 2011)
GFDL-ESM2G	(Dunne et al., 2012)
GFDL-ESM2M	(Dunne et al., 2012)
GISS-E2-H	(Schmidt et al., 2014)
GISS-E2-R	(Schmidt et al., 2014)
INM-CM4	(Volodin et al., 2010)
IPSL-CM5A-LR	(Dufresne et al., 2013)
IPSL-CM5A-MR	(Dufresne et al., 2013)
MIROC5	(Watanabe et al., 2010)
MIROC-ESM-CHEM	(Watanabe et al., 2011)
MIROC-ESM	(Watanabe et al., 2011)
MRI-CGCM3	(Yukimoto et al., 2012)

Table S3. Partial correlation coefficients between the changes in fractional coverage (FC) of NEB, BDM, BDBsh, C3Ar, C3NA, C4, and temperature (T) and precipitation (P), respectively.

	FC_{NEB}	FC_{BDM}	FC_{BDBsh}	FC_{C3Ar}	FC_{C3NA}	FC_{C4}
T	–0.89**	0.90**	–0.36	0.83**	0.64*	–0.56*
P	0.48*	0.37	–0.19	–0.57*	0.14	0.29

**Significant with *P* value less than 0.001. *Significant with *P* value less than 0.1.

Table S4. List of six regions used in this study. Only land grid points are used in the analysis.

Name	Acronym	Latitude	Longitude
Alaska	ALA	60°N–72°N	170°W–103°W
Northern Europe	NEU	48°N–75°N	10°W–40°E
Western Siberia	WSI	55°N–66°N	60°E–95°E
Eastern North America	ENA	25°N–50°N	85°W–60°W
Amazon Basin	AMZ	20°S–4°N	62°W–42°W
Southeast Asia	SEA	11°S–20°N	95°E–155°E

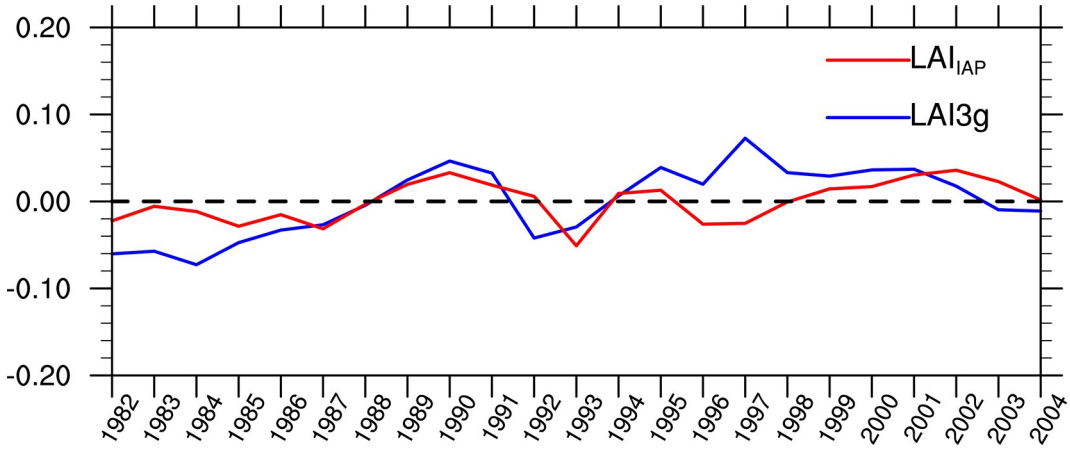

Fig. S1. The anomaly of LAI3g (blue) and LAI simulated by IAP-DGVM (red) over northern mid-high-latitudes 45°N–90°N. The linear correlation coefficient between the two lines is 0.48 (Prob<0.05, where Prob is the probability of statistical significance of the linear correlation coefficient). All units are m^2 m^{-2}.

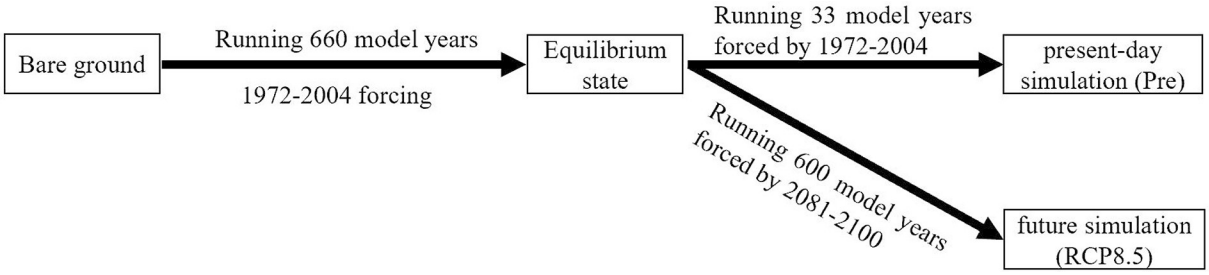

Fig. S2. Spin-up method.

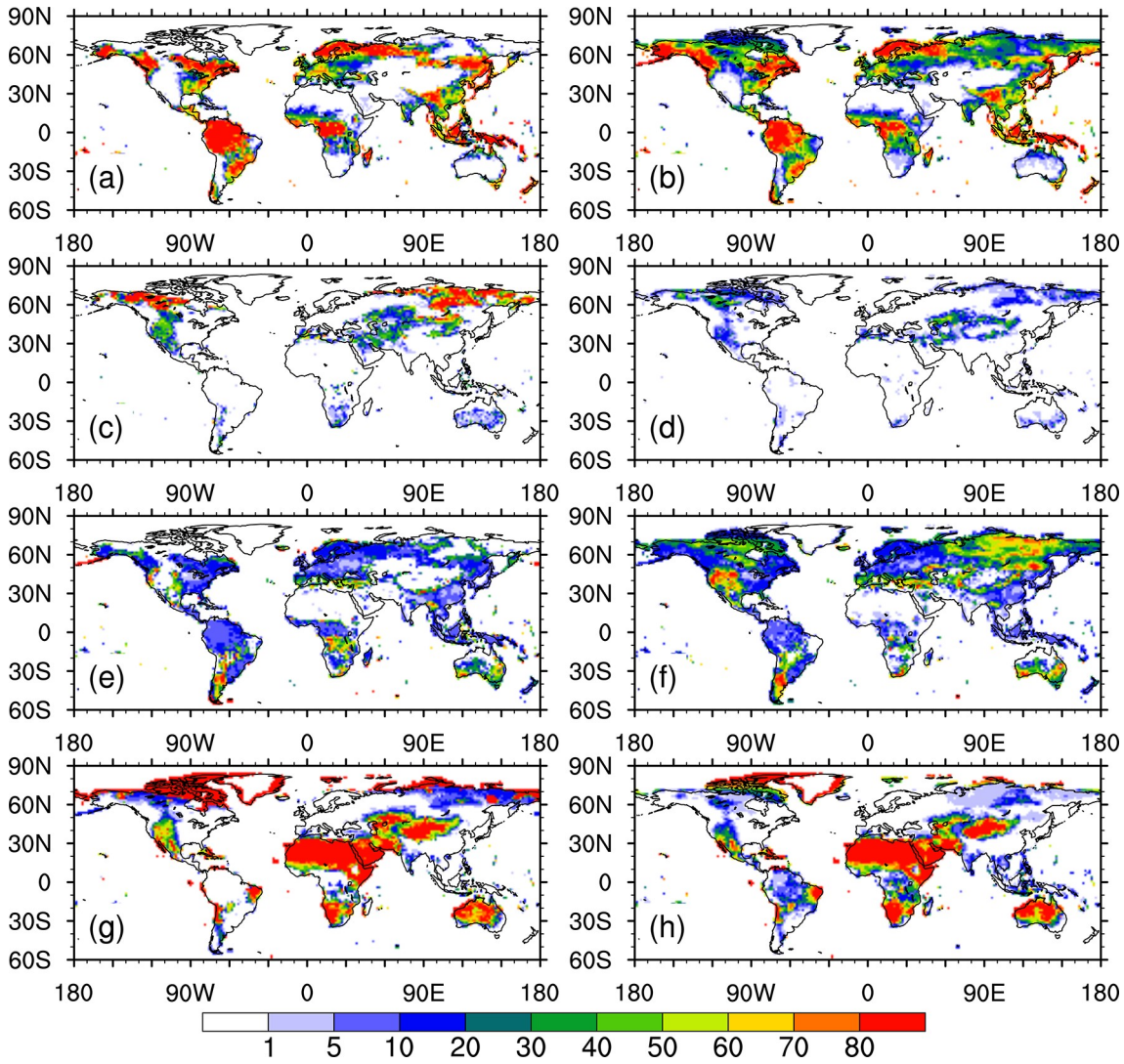

Fig. S3. Fractional coverage (units: %) of (a) trees, (c) shrubs, (e) grasses, and (g) bare ground in the present-day simulation. (b), (d), (f), and (h) are the same as (a), (c), (e), and (g), respectively, but for RCP8.5 simulations.

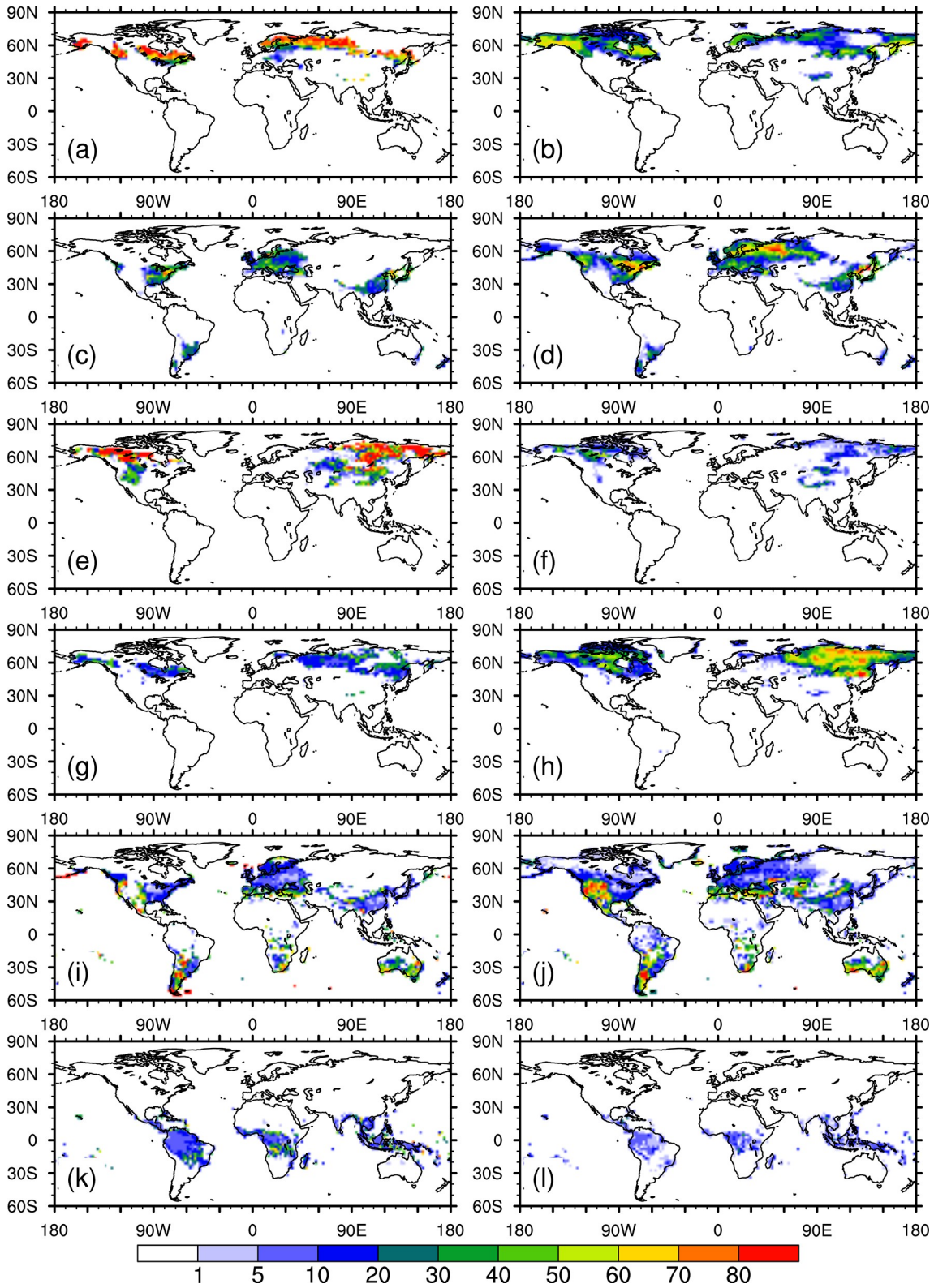

Fig. S4. Fractional coverage (units: %) of (a) NEB, (c) BDM, (e) BDBsh, (g) C3Ar, (i) C3NA, and (k) C4 in the present-day simulation. (b), (d), (f), (h), (j), and (l) are the same as (a), (c), (e), (g), (i), and (k), respectively, but for RCP8.5 simulations.

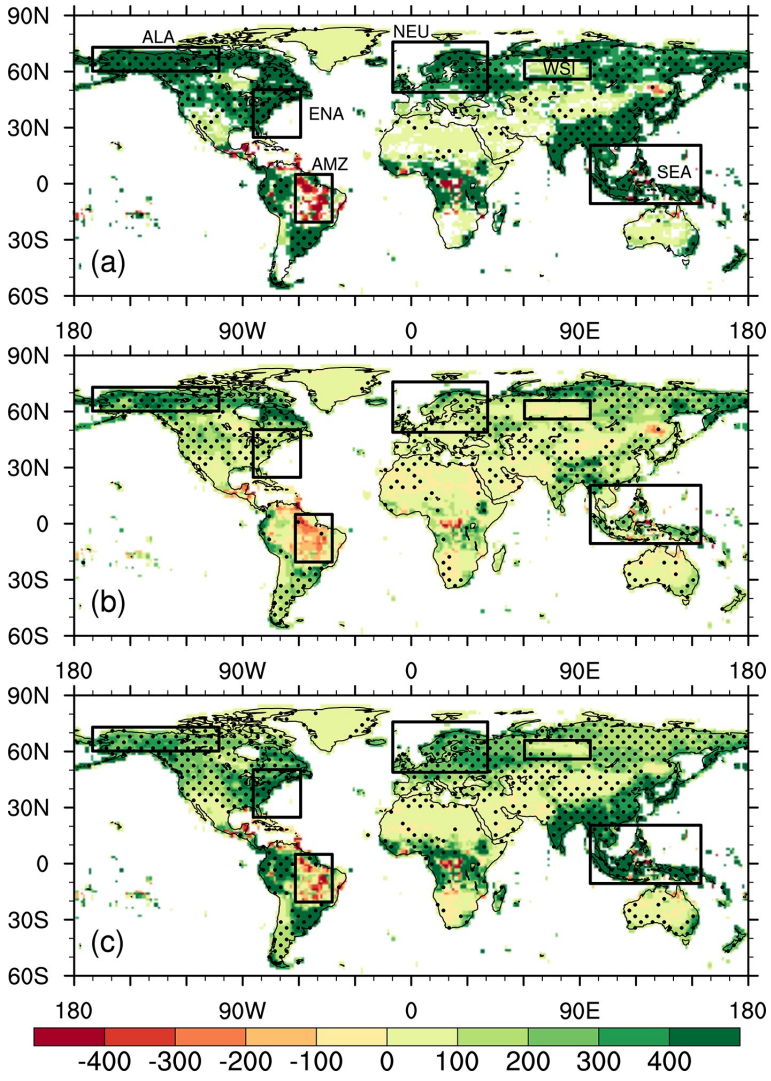

Fig. S5. The six selected regions are bounded by black rectangles in the

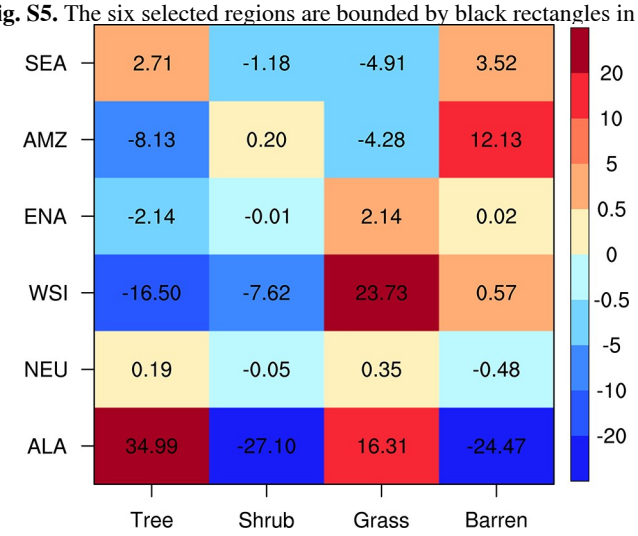

Fig. S6. Differences in fractional coverage (%) of tree, shrub, grass, and barren in the six selected regions. The y-axis represents the selected six regions that are Alaska (ALA), Northern Europe (NEU), Western Siberia (WSI), Eastern North America (ENA), Amazon (AMZ), and Southeast Asia (SEA).

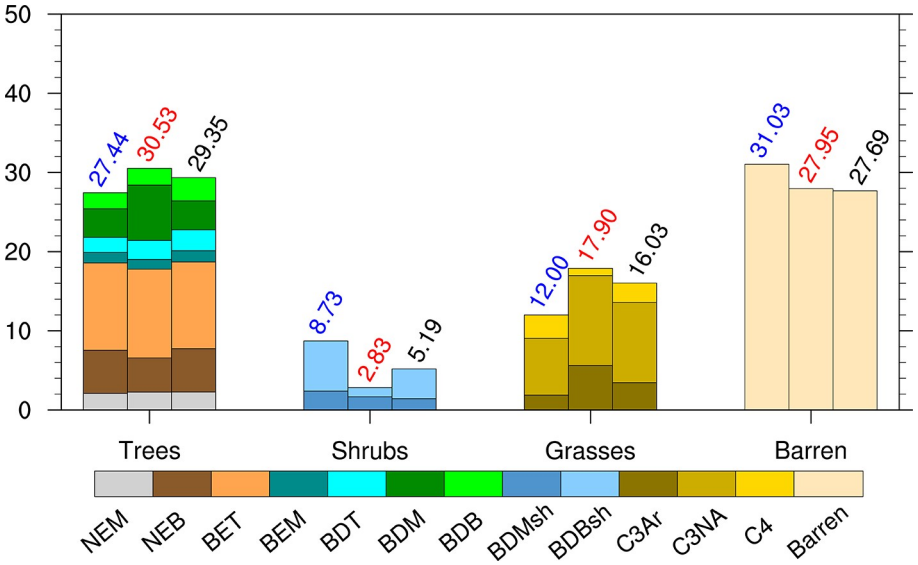

Fig. S7. Global weighted average fractional coverage (%) of each PFT for Pre (blue), RCP8.5 (red), and eCO_2 (black). The abbreviations of the PFT correspond to the information in Table S1.

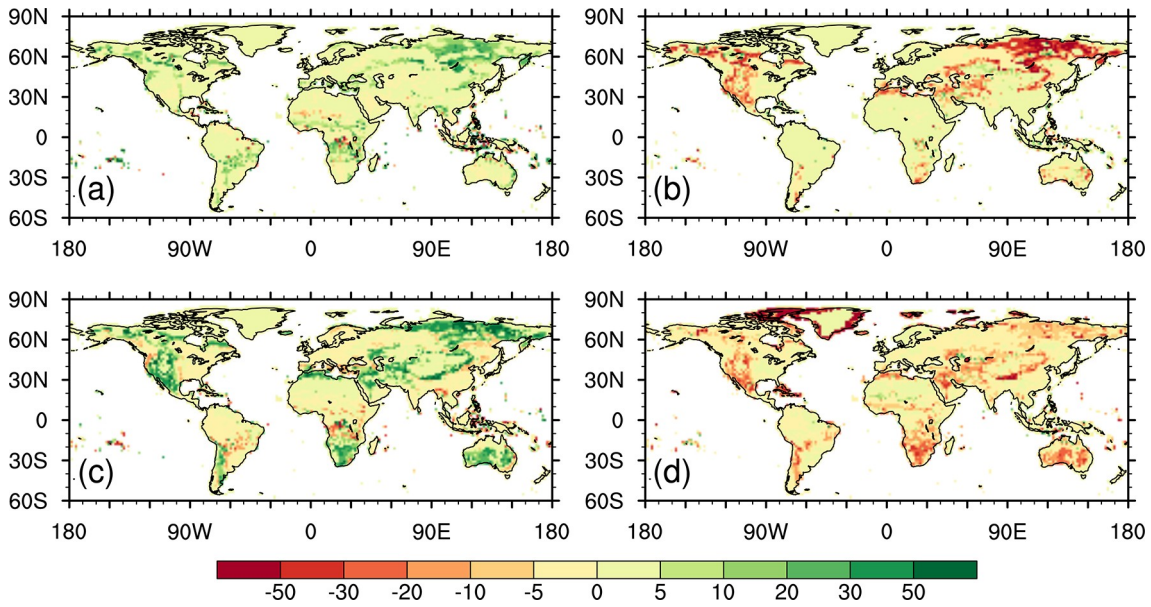

Fig. S8. Differences in fractional coverage (units: %) of (a) trees, (b) shrubs, (c) grasses, and (d) bare ground between Pre and eCO_2 (eCO_2 minus Pre).

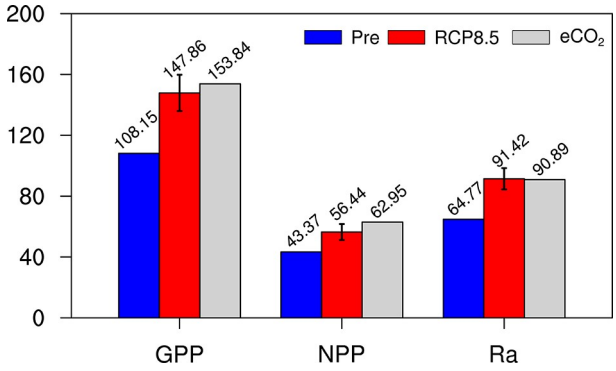

Fig. S9. Global means of carbon fluxes in Pre (blue), RCP8.5 (red), and eCO_2 (gray). The bars represent one standard deviation. All units are PgC yr^{-1}.

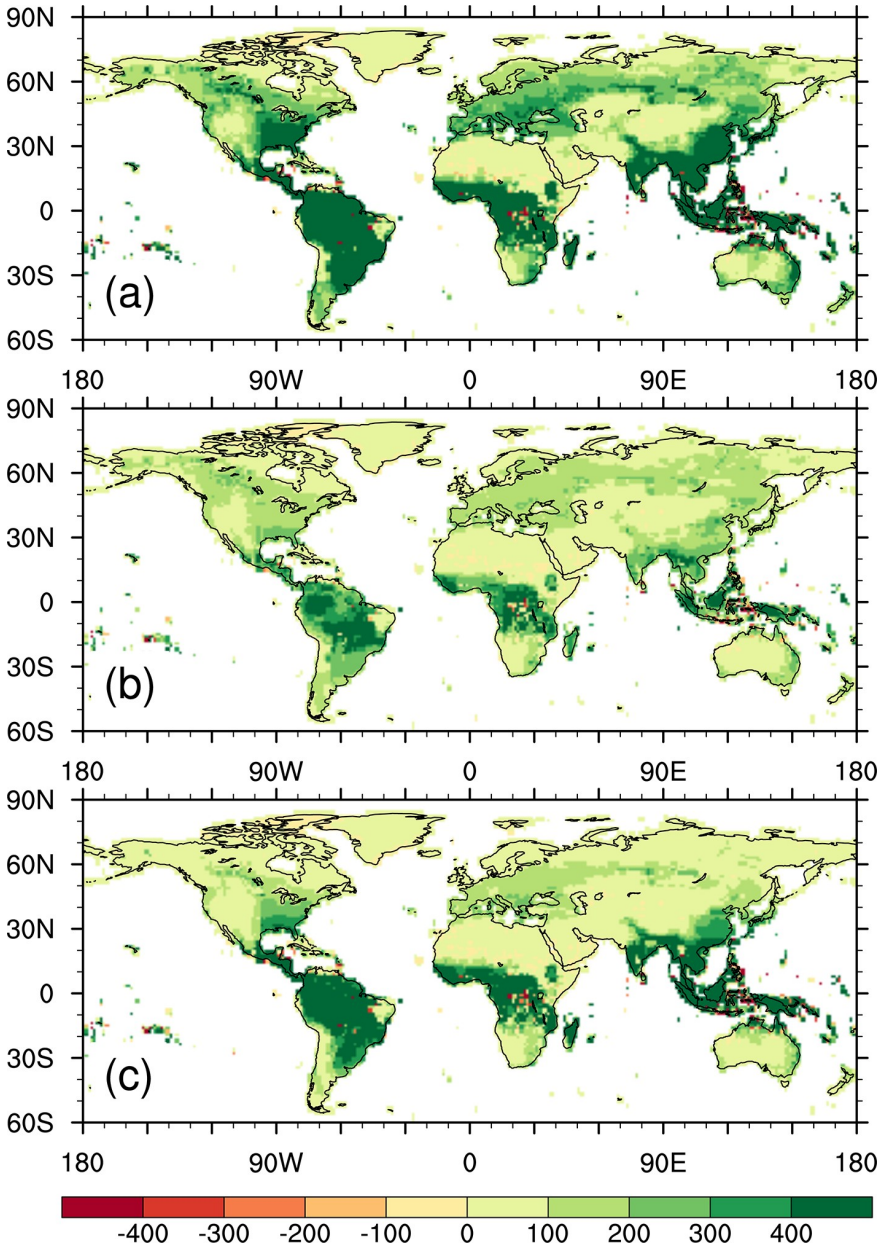

Fig. S10. Spatial distribution of differences between Pre and eCO_2 (eCO_2 minus Pre) in (a) GPP, (b) NPP, and (c) Ra. All the units are gC m^{-2} yr^{-1}.

REFERENCES

Bi, D. H., and Coauthors, 2013: The ACCESS coupled model: Description, control climate and evaluation. *Aust Met Oceanog J*, **63**(1), 41–64, https://doi.org/10.22499/2.6301.004.

Dufresne, J. L., and Coauthors, 2013: Climate change projections using the IPSL-CM5 Earth System Model: from CMIP3 to CMIP5. *Climate Dynamics*, **40**, 2123–2165, https://doi.org/10.1007/s00382-012-1636-1.

Dunne, J. P., and Coauthors, 2012: GFDL's ESM2 Global Coupled Climate–Carbon Earth System Models. Part I: Physical formulation and baseline simulation characteristics. *Journal of Climate*, **25**(19), 6646–6665, https://doi.org/10.1175/JCLI-D-11-00560.1.

Griffies, S. M., and Coauthors, 2011: The GFDL CM3 coupled climate model: Characteristics of the ocean and sea ice simulations. *Journal of Climate*, **24**(13), 3520–3544, https://doi.org/10.1175/2011jcli3964.1.

Schmidt, G. A., and Coauthors, 2014: Configuration and assessment of the GISS ModelE2 contributions to the CMIP5 archive. *Journal of Advances in Modeling Earth Systems*, **6**(1), 141–184, https://doi.org/10.1002/2013MS000265.

Voldoire, A., and Coauthors, 2012: The CNRM-CM5. 1 global climate model: description and basic evaluation. *Climate Dynamics*, **40**, 2091–2121, https://doi.org/10.1007/s00382-011-1259-y.

Volodin, E. M., N. A. Dianskii, and A. V. Gusev, 2010: Simulating present-day climate with the INMCM4.0 coupled model of the atmospheric and oceanic general circulations. *Izvestiya, Atmospheric and Oceanic Physics*, **46**(4), 414–431, https://doi.org/10.1134/S000143381004002X.

Watanabe M., and Coauthors, 2010: Improved climate simulation by MIROC5: mean states, variability, and climate sensitivity. *Journal of Climate*, **23**(23), 6312–6335, https://doi.org/10.1175/2010JCLI3679.1.

Watanabe, S., and Coauthors, 2011: MIROC-ESM 2010: model description and basic results of CMIP5-20c3m experiments. *Geoscientific Model Development*, **4**(4), 845–872, https://doi.org/10.5194/gmd-4-845-2011.

Wu, T. W., and Coauthors, 2013: Global carbon budgets simulated by the Beijing Climate Center Climate System Model for the last century. *Journal of Geophysical Research: Atmospheres*, **118**(10), 4326–4347, https://doi.org/10.1002/jgrd.50320.

Wu, T. W., and Coauthors, 2014: An overview of BCC climate system model development and application for climate change studies. *Journal of Meteorological Research*, **28**(1), 34–56, https://doi.org/10.1007/s13351-014-3041-7.